



Contents lists available at ScienceDirect

NeuroImage

journal homepage: [www.elsevier.com/locate/ynimg](http://www.elsevier.com/locate/ynimg)

# Independent encoding of grating motion across stationary feature maps in primary visual cortex visualized with voltage-sensitive dye imaging

Selim Onat<sup>a</sup>, Nora Nortmann<sup>a,b,c</sup>, Sascha Rekauszke<sup>b,c</sup>, Peter König<sup>a</sup>, Dirk Jancke<sup>b,c,\*</sup>

<sup>a</sup> Institute of Cognitive Science, Department of Neurobiopsychology, University Osnabrück, 49069 Osnabrück, Germany

<sup>b</sup> Cognitive Neurobiology, Ruhr-University Bochum, 44780 Bochum, Germany

<sup>c</sup> Bernstein Group for Computational Neuroscience, Institut für Neuroinformatik, Ruhr-University Bochum, 44780 Bochum, Germany

## ARTICLE INFO

### Article history:

Received 31 August 2010

Revised 31 December 2010

Accepted 4 January 2011

Available online xxxx

### Keywords:

Visual coding

Visual cortex

Multiplexing information

Singular value decomposition

Cortical orientation maps

Voltage-sensitive dye imaging

## ABSTRACT

In early visual cortex different stimulus parameters are represented in overlaid feature maps. Such functioning was extensively explored by the use of drifting gratings characterized by orientation, spatial-temporal frequency, and direction of motion. However surprisingly, the direct cortical visuotopic drift of the gratings' stripy pattern has never been detected simultaneously to these stationary feature maps. It therefore remains to be demonstrated how physical signals of grating motion across the cortex are represented independently of other parametric maps and thus, how multi-dimensional input is processed independently to enable effective read-out further downstream.

Taking advantage of the high spatial and temporal resolution of voltage-sensitive dye imaging, we here show the real-time encoding of position and orientation. By decomposing the cortical responses to drifting gratings we visualize the typical emergence of stationary orientation maps in which specific domains exhibited highest amplitudes. Simultaneously to these patchy maps, we demonstrate coherently propagating waves of activity that precisely matched the actual movement of the gratings in space and time, most dominantly for spatial frequencies lower than the preferred range. Thus, the primary visual cortex multiplexes information about retinotopic motion by additional temporal modulation of stationary orientation signals. These signals may be used to variably extract coarse-grained object motion and form information at higher visual processing stages.

© 2011 Published by Elsevier Inc. 40

## Introduction

Fifty years ago, neurons in primary visual cortex were discovered to have local receptive fields that are selective for stimulus orientation (Hubel and Wiesel, 1959). Moreover, it has been found that neurons are grouped systematically across the cortical plane representing visual space and contours in overlaid retinotopic and orientation maps (Hubel and Wiesel, 1974). Intrinsic optical imaging revealed further details of the distinct cortical functional organization establishing the columnar arrangement of ocular dominance, motion direction, and spatio-temporal frequency maps (Blasdel and Salama, 1986; Bonhoeffer and Grinvald, 1991; Bosking et al., 1997; Hübener et al., 1997; Shoham et al., 1997; Xu et al., 2006). But how are these different information channels efficiently encoded across large neuronal populations without undesirable interferences?

In primary visual cortex the precise temporal structure of the neuronal spike patterns in the gamma range [40–80 Hz] was proposed as a fundamental mechanism to enable binding as well as segmentation of visual features (Abeles, 1991; Gray et al., 1989), in addition to mechanisms in which amplitudes of instantaneous firing rates of coactive neurons (Roelfsema et al., 2004), or entire spike trains (Jancke, 2000; Richmond et al., 1990), all play an important role in processing (Kayser et al., 2009). Intrinsic optical imaging research to date shows that moving gratings – as a means to provide simultaneous multi-dimensional visual input – are cortically represented by unique patchy activity patterns where the locations of the activated domains are interpreted to either reflect the intersection of orientation, spatial frequency, and direction maps (Blasdel and Salama, 1986; Bonhoeffer and Grinvald, 1991; Bosking et al., 1997; Hubel and Wiesel, 1974; Hübener et al., 1997; Shoham et al., 1997; Xu et al., 2006), or to encode the overall spatio-temporal energy of these features (Basole et al., 2003; Mante and Carandini, 2003; see Issa et al., 2008 for recent review). In either case, since multiple feature combinations can produce an identical stationary map (Basole et al., 2003) its information content remains ambiguous (Movshon et al., 1985; Rust et al., 2006; Zhang and Britten, 2006). Particularly in the event of moving gratings such feature map fails to additionally

Abbreviations: VSD, voltage-sensitive dye; SVD, singular-value decomposition.

\* Corresponding author. Bernstein Group for Computational Neuroscience, Institut für Neuroinformatik ND 03/70, Ruhr-Universität Bochum, Universitätsstr. 150, D-44780 Bochum, Germany. Fax: +49 234 32 14209.

E-mail address: [jancke@neurobiologie.rub.de](mailto:jancke@neurobiologie.rub.de) (D. Jancke).

capture the physical motion of the grating across the retinotopic representation and therefore, neglects the permanent space–time changes in luminance caused by the gratings' stripes. Instead, given that retinotopy is independent of orientation (Bosking et al., 2002; Buzas et al., 2003; Yu et al., 2005, but see Das and Gilbert, 1997), smoothly traveling waves of activity (Engel et al., 1994, 1997; Lee et al., 2005) should be detectable at the same time.

However, the applied recording methods so far were limited in sampling: single electrode recordings hamper a coherent population picture of activation across the cortex due to restrictions in spatial sampling, whereas intrinsic optical imaging is limited in temporal resolution because of its dependence on slow hemodynamic processes. Also with fMRI, as another method that uses hemodynamic signals, retinotopic waves and orientation maps were never captured simultaneously (Yacoub et al., 2008). To overcome these limitations, we made use of an imaging technique that employs voltage-sensitive dye to record population activity in the millisecond range across several millimeters of cat visual cortex with high resolution (Grinvald et al., 1994; Jancke et al., 2004; see Grinvald and Hildesheim, 2004 for review).

## Materials and methods

We recorded from cat primary visual cortical area spanning A17 and A18 (11 animals, 12 hemispheres). Detailed analysis was performed in 6 experiments, in which the compound spatio-temporal activity was found. Standard surgical and experimental procedures were used, approved by the German Animal Care and Use Committee (AZ 9.93.2.10.32.07.032) in accordance with the Deutsche Tierschutzgesetz and NIH guidelines.

### Animal preparation

Animals were initially anesthetized with ketamine (15 mg kg<sup>-1</sup> i.m.) and xylazine (1 mg kg<sup>-1</sup> i.m.), supplemented with atropine (0.05 mg kg<sup>-1</sup> i.m.). After tracheotomy, animals were artificially respirated, continuously anesthetized with 0.8–1.5% isoflurane in a 1:1 mixture of O<sub>2</sub>/N<sub>2</sub>O, and fed intravenously. Heart rate, intratracheal pressure, expired CO<sub>2</sub>, body temperature, and EEG were monitored during the entire experiment. The skull was opened above area 17/18 and the dura was resected. Paralysis was induced and maintained by Alloferin®. Eyes were covered with zero-power contact lenses as protectives. External lenses were used to focus the eyes on the screen. To control for eye drift, the position of the area centralis and receptive field positions were repeatedly measured. A stainless steel chamber was mounted and the cortex was stained for 2–3 h with voltage-sensitive dye (RH-1691), and unbound dye was subsequently washed out.

### Stimulus presentation

Gratings (0.1/0.2/0.4 c/deg, 6.25 Hz) were presented on a Monitor (100 Hz, mean luminance 11 cd m<sup>-2</sup>, Sony Triniton GDM-FW900, Japan) covering a visual field of 30×40°. To detect the area 17/18 border, gratings of 0.6 c/deg and 2 Hz were used. Eyes were converged using a prism. Stimuli were randomly displayed for 2 s (including

200 ms of prestimulus duration), followed by a uniform gray screen (blank condition) presented for 15 s during the interstimulus intervals.

### Data acquisition and pre-processing

Optical imaging was accomplished using an Imager 3001 (Optical Imaging Inc, Mountainside, NY) The camera was focused ~400 nm below the cortical surface. Data acquisition onset was synchronized with heart-beat signal. For detection of changes in fluorescence the cortex was illuminated with light of 630 ± 10 nm and emitted light was high-pass filtered with a cut-off of 665 nm (camera frame rate 220 Hz). Divisive normalization was performed by dividing each pixel value by its DC level during 200 ms pre-stimulus time (in which a uniform gray screen was presented); heart-beat and respiration-related artifacts were removed by subtracting the average blank signal.

### Singular value decomposition analysis

Evoked signals were computed by averaging 25 to 50 stimulus repetitions. For singular value decomposition (SVD) analysis we chose the time interval in which activity roughly stabilized (>400 ms). Technically, the entire time course or a time window starting closer to response onset could be used. However, inclusion of the transient response part, characterized by huge changes in overall activity, reduces sensitivity of the method to the later oscillatory part of the responses. We applied SVD to the evoked activity by using *svd* command of Matlab software (Mathworks, Natick, MA, USA) after transforming each frame into a vector. SVD transforms the data matrix representing the evoked signal,  $S(t,x)$ , into a weighted sum of  $N$  space–time separable matrices,  $g_i(t,x)$ , such that  $S(t,x) = \sum_i^N g_i g_i(t,x)$ ; where  $g_i$  represents the weight of the  $i$ th modes and  $N$ , the number of frames. The matrix  $g_i(t,x)$  can be described as the outer product of two vectors  $u_i(x)$  and  $v_i(t)$  representing the  $i$ th spatial and temporal modes. Interpreting the rows of  $S(t,x)$  as samples and the columns as features  $u_i(x)$  and  $v_i(t)$  are the eigenvectors of the sample and feature covariance matrices i.e. principal components, respectively. Singular values,  $g_i$ , increased linearly with logarithmic scale and significant components were detected by identifying the first component with significant increase in its weight with respect to the previous components. To selectively reconstruct the oscillatory activity, we selected those components with a prominent peak at the required frequency. In some cases fitting harmonic functions to the temporal modes at the required frequency beforehand improved the results.

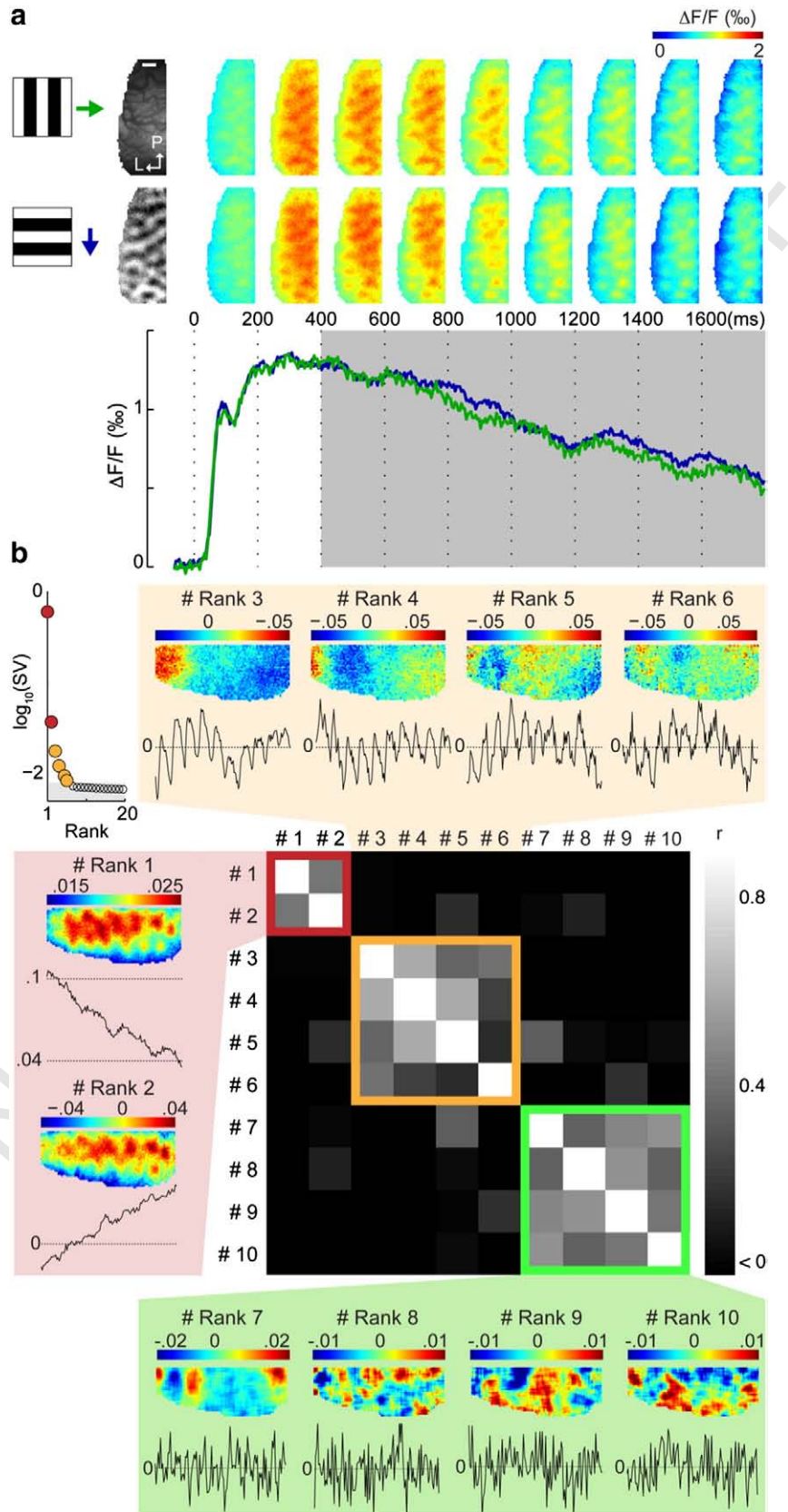
## Results

Cortical responses to drifting gratings were measured that moved either rightwards or downwards across the contra-lateral visual field (Fig. 1a). These stimuli give rise to complementary activity pattern as demonstrated by the difference map (Fig. 1a, second row, leftmost). The lower graph in Fig. 1a shows the evoked time courses of activity of one experiment averaged across the imaged region for each grating direction. Activity rises steeply after stimulus onset, suspended by an

**Fig. 1.** Decomposition of evoked cortical responses to gratings of 0.2 c/deg drifting for 2 s at a temporal frequency of 6.25 Hz. (a) Evoked spatio-temporal activity patterns (top rows) and time courses obtained by spatial averages across the images (bottom traces) expressed as fractional change in fluorescence relative to blank condition ( $\Delta F/F$ ). Top left frame shows the vascular image of the recorded right hemisphere, P = posterior, L = lateral; here and in all figures scale bar 1 mm. Leftmost frame in 2nd row depicts the time-averaged orientation map derived by subtracting evoked responses to the vertical grating from horizontal. Green trace = responses to vertical grating, drifting rightwards in visual space; blue trace = horizontal grating, drifting downwards. (b) Top left corner, singular values,  $g_i$ , ranked in order of their contributions. Components of significant contribution to variance are colored (gray area depicts significance level). The contribution of each single SVD component to single recorded trials ( $n = 35$ ) was computed, their correlations across trials are represented as a matrix. Spatial ( $u_i(x)$ ) and temporal ( $v_i(t)$ ) modes of the SVD components were clustered according to their correlation (red, yellow, and green boxes; curves represent weight of each spatial mode [ $y$ -axes] as a function of time [400–1800 ms]). (For interpretation of the references to color in this figure legend, the reader is referred to the web version of this article.)

180 intermediate deceleration–acceleration notch after ~85 ms (Sharon  
 181 and Grinvald, 2002), reaching maximum levels after 300 ms, followed  
 182 by a slow monotonic decay.

Singular-value decomposition (SVD) was applied to the later part of  
 the evoked responses (Fig. 1a, gray area in bottom traces, 400–1800 ms)  
 excluding the fast transient onset (see Material and methods, SVD



analysis). SVD decomposes the evoked signal into distinct orthonormal components that are separable into their spatial and temporal modes. The relative importance of each component, i.e. fraction of variance explained, is captured by the size of the singular value (Fig. 1b, top-left). We observed 6 significant singular values spanning a range of two orders of magnitude. This shows that the responses to gratings are characterized by compound dynamics that result in spatio-temporal inseparability of activity.

To infer the biological significance of the SVD components we reasoned that the contributions of individual components must exhibit co-variation across trials. Indeed, the respective correlation matrix revealed different clusters of SVD components (Fig. 1b). The first cluster encompasses two SVD components with highest singular values, each displaying non-oscillatory tonic activity modes (Fig. 1b, red/left). This was observed in all measured hemispheres. The second cluster included 4 SVD components with smaller singular values and strong oscillatory activity (Fig. 1b, orange/top) matching the fundamental frequency of the moving grating (6.25 Hz). For the present example, additional SVD components followed (Fig. 1b, green/bottom) displaying distinct oscillations at the 2nd harmonic of the grating's temporal frequency. We found that these oscillatory dynamics were almost exclusively accounted for by those higher order SVD components that did not have orientation selective spatial modes (see Fig. 2a for average power spectra across the significant temporal modes and Fig. 2b for relationship between their oscillatory strength and orientation selectivity across all experiments).

Reconstruction of activity using the first cluster of SVD components displayed the typical patchy structure of stationary orientation maps characterized by repeating local domains of peak amplitudes (Fig. 3, see contours in red panels, first and third rows). The regions maximally activated by the different orientations are largely non-overlapping resulting, as expected, in orthogonal maps of activation (Supplementary Material Fig. S2). Bear in mind that other stimulus dimensions are mapped within primary visual cortex as well. For example, regions differ in their responsiveness to stimuli of different spatial frequency (Shoham et al., 1997). Yet, orientation maps determined by gratings of different spatial-temporal frequencies are highly overlapping (Supplementary Material Fig. S3). Thus, we conclude that in the present experiment the response captured by the first cluster of SVD components is dominated by the orientation selectivity of neurons in primary visual cortex.

Overlaid on these maps, the second cluster of oscillatory SVD components (orange panels/second and fourth rows) revealed cyclic

waves of activity that propagated either medial to lateral (right to left in image frames) or in posterior–anterior direction (from top downwards) across the cortex depending on the gratings' drifting direction. Evidently, the retinotopic propagation was not restricted to particular regions as it passed coherently through both preferred orientation and orthogonally tuned domains (see also Supplementary Material Movie 1; Movie 2 shows an opposite left hemisphere in which the rightwards drifting grating produced the expected propagation in opposite direction). Moreover, the fact that these waves propagated with the same temporal frequency as the grating suggests an underlying asymmetry in the responses to its dark and bright stripes (see Discussion). In addition, the higher order SVD components (7 to 10) exhibited waves of half spatial wavelength, thus reporting the individual contrast changes at each of the grating edges (Fig. 3, last row).

We next extracted the phase of the best fitting harmonic functions (Fig. 4a) for each pixel and plotted these values topographically (Fig. 4b). The change in phase as a function of cortical distance resulted in values of ~30 and ~39 mm/s (for medial–lateral and anterior–posterior direction, respectively). Given the speed of the drifting gratings (~31 deg/s) this cortical propagation speed matches to the known magnification factor of the central visual field representation of area 17 (Tusa et al., 1978). Hence, overall the oscillatory SVD components reflected the shifts of the gratings' stripes with high spatial and temporal accuracy. Notably in this experiment the signal-to-noise ratio of the propagating waves was highest medial to the 17/18 areal border (Fig. 4b, see dashed white lines in the respective phase plots, and Supplementary Material Fig. S4). However, when a grating of lower spatial frequency (0.1 c/deg) was used in another experiment, propagation was evoked concurrently across both primary visual areas (Fig. 4e; see Supplementary Material Fig. S5 for space–time diagram). We calculated the power of the oscillatory components dependent on the grating spatial frequency for each area 17 and 18 separately. At all spatial frequencies investigated, oscillatory power in area 17 was higher than in area 18 (Fig. 4f), on average by a factor of 1.7. This may suggest that the emergence of retinotopic grating propagation is area specific and might lead to the situation where the retinotopic component is independently processed in area 17 while in area 18 such multiplexing is absent or weak.

We additionally explored further systematic variations of the gratings' spatial frequency and drifting direction in this experiment (Fig. 5). The highest spatial frequency measured (0.4 c/deg) evoked activity with principle oscillation matching the grating temporal

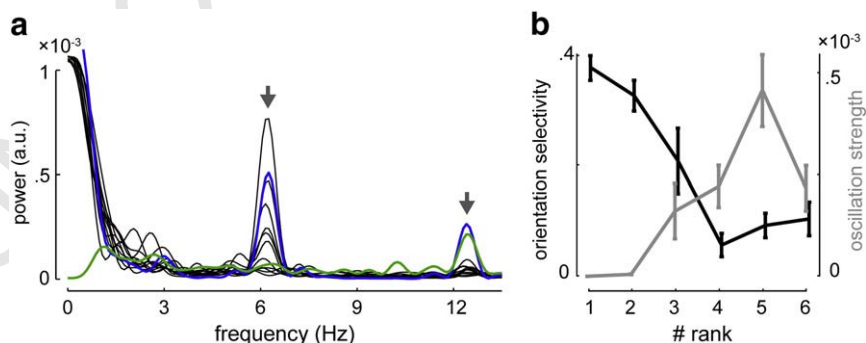


**Fig. 2.** (a) Power spectra of temporal modes averaged across significant components for all experiments (black lines). In 6 of 12 hemispheres a prominent peak at 6.25 Hz was observed (see arrowhead). For the experiment presented in Fig. 1, components 7 to 10 were characterized by another prominent peak at 12.5 Hz (green line, see 2nd arrowhead). Blue line depicts spectrum characteristics of responses to a grating of lower spatial frequency (0.1 c/deg, cf. Fig. 5, bottom rows). (b) Orientation selectivity of spatial modes (black line) and power at 6.25 ± 1 Hz (gray line) are shown for the first 6 SVD components across all experiments. Orientation selectivity was evaluated by quantifying the correlation between spatial modes and differential orientation map (shown in Fig. 1a). Power at 6.25 Hz (± 1.00 Hz) was computed for each component. Differences in the singular values were accounted by weighting each component's power by its singular value. With increasing rank the power at 6.25 Hz increased while the correlation of the spatial modes to the orientation maps decreased. Error bars indicate SEM. As a control, we additionally compared the power at 6.25 (± 1.00 Hz) to a baseline (i.e. power at flanking frequencies, 3.25 Hz–5.25 Hz and 7.25 Hz–9.25 Hz). For the first cluster (components 1 to 2) the power at 6.25 Hz was on average 1.21 ± 0.18 times higher, but was increased by a factor of 8.63 ± 1.56 for the second cluster (components 3 to 6), indicating that oscillatory components were almost independent from cortical representation of orientation. (For interpretation of the references to color in this figure legend, the reader is referred to the web version of this article.)

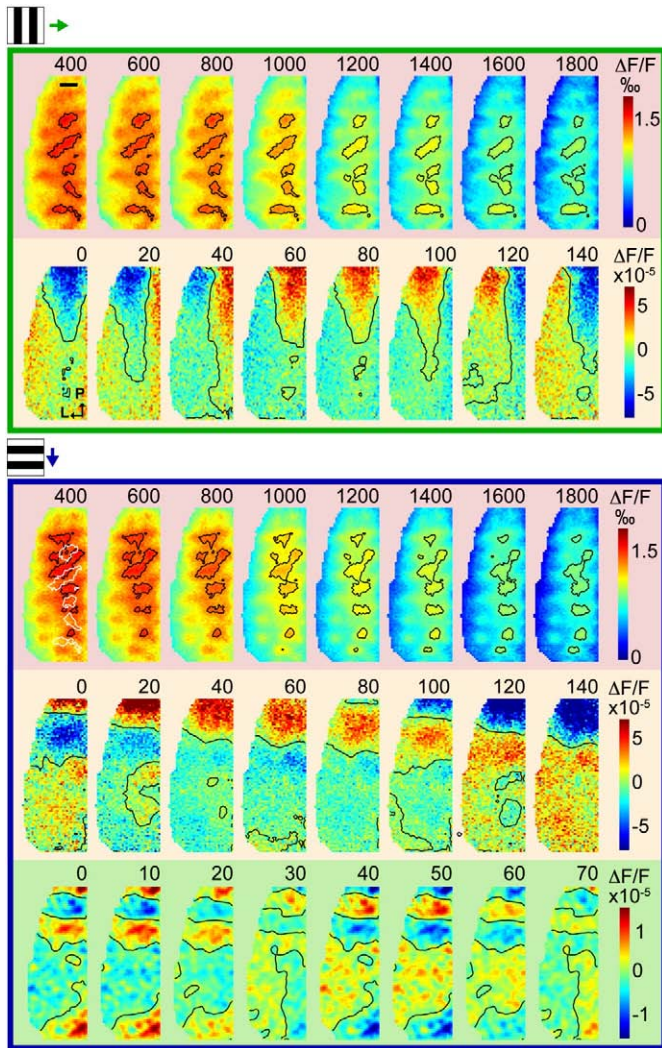


**Fig. 3.** Propagation of retinotopic cortical activity across stationary orientation maps. Icons on top sketch stimulus conditions. Within each panel, spatio-temporal activity dynamics represented by different SVD components are shown (color code as in Fig. 1b): tonic components (red panels, top rows), oscillatory components with principle oscillation frequencies at 6.25 (orange panels, second rows) and 12.5 Hz (green panel, bottom row). Time after stimulus onset (red panels) or relative to the propagation period (orange and green panels) is indicated above each single frame. Note the difference in the time-scales. To capture a full cycle of propagating activity, only a single period (duration 160 or 80 ms) is depicted (multiple cycles were averaged, see Supplementary Material Movie 1). Contour lines are drawn around 90th percentiles of activity for the tonic components (contours in first frame of upper box were copied as white outlines to first frame in lower box for comparison) and at zero crossings for the oscillatory components. Color bars depict activity levels,  $\Delta F/F$ ; note the two-order difference in amplitudes between the two scales. See Supplementary Material Fig. S1 for rough retinotopic sampling of the imaged cortical area using electrophysiology. (For interpretation of the references to color in this figure legend, the reader is referred to the web version of this article.)

287 frequency. However, the retinotopic modulations of these waves were  
 288 less pronounced, which could be due to limitations in the spatial  
 289 resolution of our method or caused by likely differences in physiological  
 290 mechanisms (Movshon et al., 1978a,b). Wave amplitudes and retino-  
 291 topic spatial resolution increased then systematically with lower spatial  
 292 frequencies (Fig. 5, top to bottom). Importantly, a sinusoidal grating  
 293 (0.2 c/deg) showed comparable propagation characteristics as a square-  
 294 wave grating of equal spatial frequency (Fig. 5, second and third row,  
 295 respectively. Note that the third row represents an oblique grating).  
 296 With lower spatial frequencies of the gratings (0.1 c/deg, Fig. 5 bottom  
 297 rows), additional SVD components with power at 12.5 Hz, representing  
 298 each grating edge, became increasingly significant (Fig. 5, last row).

## Discussion

299

We have demonstrated how the primary visual cortex – as the  
 cortical bottleneck along the visual pathway – disambiguates two  
 parameters, visual space and orientation: Besides representation of  
 stationary orientation maps we show additional response components  
 that simultaneously signal retinotopic grating motion through small  
 oscillatory modulations of synaptic activity. Thus, our study demon-  
 strates for the first time directly, how retinotopic millisecond  
 propagation of grating motion is represented across stationary feature  
 maps. We found that only a small portion of the entire signal amplitude  
 represents such physical motion. Importantly, these retinotopic waves  
 were homogeneously traversing the orientation maps indicating inde-  
 pendent and parallel multiplexing of the retinotopic signals.

### Sources of the optical signal

312

The dye signals in cortical responses to visual stimulation are  
 commonly of amplitudes in the range of maximal 2% relative to  
 baseline fluorescence levels (Grinvald and Hildesheim, 2004; Jancke  
 et al., 2004; Sharon and Grinvald, 2002; Sharon et al., 2007). The  
 oscillatory signal reported here was even two orders of magnitude  
 lower and only detectable in our highest quality recordings as the  
 functional signal is most sensitive to various sources of noise  
 (Grinvald and Hildesheim, 2004; Reynaud et al., 2011). Besides  
 noise due to heart-beat pulsations and breathing artifacts (Grinvald  
 and Hildesheim, 2004), which were largely eliminated by our data  
 recording and processing procedures, shot-noise induced by statisti-  
 cal fluctuations of the light emitting process is a major technical  
 obstacle to detect small activity changes. Therefore, the intensity of  
 staining, i.e. baseline fluorescence levels, should ideally be as high as  
 possible (Grinvald et al., 1988; Ross et al., 1977). However, such  
 requested high levels of staining are not achievable in all preparations  
 and consequently, recordings of the oscillatory components were not  
 revealed in every experiment. Thus, the limiting factor here is most  
 likely of technical origin rather than reflecting a genuine physiological  
 variability across animals.

Extra-cellular recordings performed in parallel to the optical  
 measurements confirmed that high amplitudes of the dye signal  
 corresponded to spiking cortical activity. Yet, we cannot estimate the  
 relative contribution of various cell types as the optical signal captures  
 activity of a large pool of neurons. Most likely the oscillatory signal is  
 dominated by complex cells, since simple cell activity is phase  
 dependent and may therefore be cancelled out at the population level  
 where phases are arbitrarily mixed (Benucci et al., 2007). Moreover,  
 VSD imaging emphasizes activity in upper cortical layers 2/3  
 (Petersen et al., 2003) and therefore highlights intra-layer propaga-  
 tion of activity via long-range horizontal connections, including  
 subthreshold postsynaptic cortical activation (Jancke et al., 2004).

The amplitudes of the retinotopic waves detected here were most  
 prominent when the grating's spatial frequency was at the lower end  
 of the known bandpass characteristics of neurons in the respective  
 visual area (Movshon et al., 1978b). This suggests that the relative  
 width of the grating period plays a critical role for the emergence of  
 the retinotopic waves (Maffei and Fiorentini, 1973; Movshon et al.,  
 1978a). In view of the high power at the fundamental, compared to  
 double temporal frequency, these retinotopic waves may result from  
 an asymmetry in the responses to dark and bright (Jin et al., 2008).  
 Indeed, a recent study in macaque primary visual cortex (V1) showed  
 that neuronal responses in layers 2/3 (the layers our method is most  
 sensitive to) was higher to "black" as compared to "white" stimuli  
 (Yeh et al., 2009). Consequently, a traveling wave may emerge from  
 units that are periodically driven by the gratings' dark edges.  
 However, oscillatory signals were also evident for sinusoidal gratings  
 devoid of sharp edges, for higher spatial frequencies (0.4 cycles/deg)  
 close to the preferred range of area 17 (Pollen et al., 1978), and

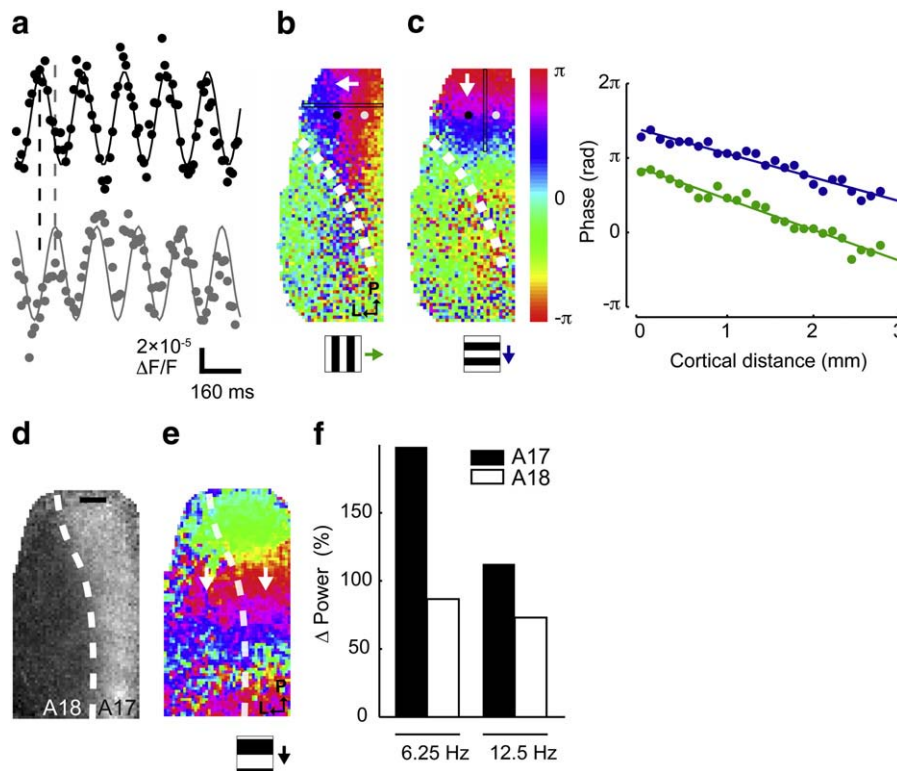


**Fig. 4.** Phase vs. space: propagation speed of cortical activity. (a) Oscillatory activity around two pixels separated by 1 mm along the medial–lateral axis (gray and black dots in panel (b)). Oscillatory activity was best described by a harmonic function with a period of 160 ms (black and gray fitted curves). (b) The phase of each pixel is shown topographically for both grating conditions. Estimate of A17/18 border is shown as stippled line. Arrows indicates direction of motion. (c) Change of phase as a function of space within circumscribed regions (see vertical and horizontal rectangles in (b)). The slope of the fitting lines was on average across both propagation directions  $\sim 1.2$  radians per mm. (d) Another experiment (right hemisphere) where the A17/18 border was mapped with gratings of 0.6 c/deg. Stippled line delineates at 75th percentile. (e) Phase map computed from oscillatory components in response to a downward drifting grating of 0.1 c/deg spatial frequency. (f) Increase of oscillatory power in A17 and A18 in percentage of baseline power at 6.25 Hz and 12.5 Hz across all conditions.

uniformly encompass regions of preferred and opposite orientation selectivity. Altogether these observations indicate that the periodic drive constitutes the main but not necessarily the full explanation of the current findings. Also top-down influences may be involved (Ahmed et al., 2008) thus, further studies are needed to identify the various possible mechanisms contributing to retinotopic grating propagation.

#### Space–time inseparable dynamics revealed by SVD analysis

In general, SVD and other directly related procedures such as principal component analysis (PCA or Karhunen–Loève transform) are analytical matrix decomposition methods. SVD and related statistical procedures are thus helpful mathematical tools to separate spatial patterns given by eigenvalues of the autocorrelation matrix from temporal modes in complex physical systems (Aubry et al., 1991; Sirovich, 1987). Such procedures were also successfully applied in waveform analysis of evoked neuronal potentials (Glaser and Ruchkin, 1976) and spike response patterns (Abeles and Goldstein, 1977). In a first attempt to model optical imaging data by Karhunen–Loève decomposition, different modes could be identified that resembled the layout of intrinsically recorded maps of ocular dominance, orientation, and direction in primary visual cortex (Sirovich et al., 1996). PCA is based on the correlations that exist in the multidimensional data and describes it in a new coordinate system where the basis vectors are linearly decorrelated and ranked in descending order according to the explained variance. SVD (or temporal PCA) extends the PCA and explains the data as weighted sums of space–time separable matrices, where the temporal and spatial modes correspond to principal components. The SVD algorithm is therefore mathematically equivalent to applying PCA in a specific form to spatial and temporal dimensions

(Sornborger et al., 2003; Strang, 2007; see Material and methods, Singular value decomposition analysis section). In the simplest case, where the responses are space–time separable, the dynamics can be described as the outer product of temporal and spatial modes. In the presence of strong space–time correlations the outer product fails to account for the full variance. However, the residuals can be subject to the same analysis, successively explaining the remaining dynamics. SVD implicitly iterates this process and describes the data with a finite sum of products of temporal and spatial modes. Specifically, the algorithm refers only to the covariance matrix and not to higher order moments. Another decomposition method, independent component analysis (ICA) takes a completely different approach. It describes the dataset in a coordinate system where statistical dependencies between different dimensions are minimal. For example, it has been proven useful in cleaning EEG recordings of biological artifacts like heart-beat and eye movements (Jung et al., 2000). An important aspect of ICA is that the number of sources that are responsible for generating the observed data has to be fixed and the precise choice affects the final solution. In the present case the number of generators is not a priori known. Therefore, SVD in the present context seems to be better suited to analyze our data. Earlier SVD analysis of VSD recordings in the turtle visual brain led to discovery of rich dynamics of widespread traveling activity in different low frequency bands < 5, 10, and 20 Hz (Prechtl et al., 1997). Such large-scale timing differences of complex activity patterns across the brain were speculated to reflect processing of diverse visual features by multiple phases of neural activity (Prechtl et al., 1997; Senseman and Robbins, 1999).

In this cortical study, the stimulus was a simple constantly drifting grating. Its orientation was encoded by tonic and highest response amplitudes across cortical neurons located in specific orientation domains. In addition, the gratings' actual motion was represented by

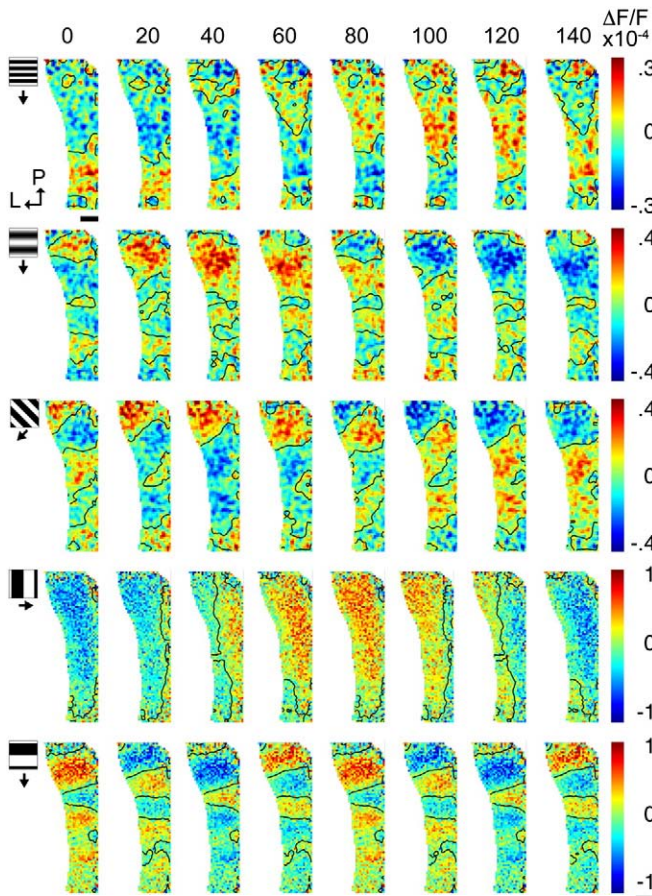


**Fig. 5.** Retinotopic propagation of cortical activity in response to gratings varying spatial parameters. SVD components with principle oscillation at either 6.25 Hz (rows 1–4) or 12.5 Hz (last row) were used to reconstruct the oscillatory dynamics in A17 (as outlined in Fig. 3D). Icons at left sketch the different grating conditions from top to bottom: 0.4 c/deg, 0.2 c/deg (sinusoidal), 0.2 c/deg (oblique), 0.1 c/deg (vertical and horizontal). Modulation amplitudes were highest for low frequency gratings. Note the systematic change in propagation direction and spatial wavelength of activity. Contour lines are drawn at zero crossings. Color bars depict activity levels,  $\Delta F/F$ . (For interpretation of the references to color in this figure legend, the reader is referred to the web version of this article.)

stimulus locked propagation of activity for which the relative timing reflected local movement of the gratings' stripes across the retinotopic map independent of orientation domains (Bosking et al., 2002; Buzas et al., 2003; Yu et al., 2005). This observation has an important implication for orientation selectivity: The fact that the propagating waves do not omit orthogonal orientation domains suggests that orientation tuning is influenced by non-orientation specific thalamic or intracortical inputs and consequently, affected through amplitude modulations representing visual space. As a result, non-specific parts of the orientation tuning curve may indeed contain residual retinotopic related activity in response to non-preferred orientations.

#### Multiplexing of visual information at different spatio-temporal scales

Along the visual pathway multiplexing of oscillatory signals is a general way to increase the amount of information being transmitted (Koepsell et al., 2010). Multiplexed channels acting across various time scales were recently also observed at the subcortical level in thalamic spike trains (Koepsell et al., 2009). The authors found that the firing rate at low frequencies encoded local changes of the stimulus. The second channel, in the gamma frequency range, was coupled to retinal oscillations. It was concluded that these higher frequencies possibly transmit global visual features. However, which frequency band encodes which parameter might critically depend on

the stimulus characteristics and on the visual task (Ahissar and Arieli, 2001). For instance, fixational eye movements, which are naturally accompanied by incessant jitter, improve discrimination of local fine spatial details within a visual scene by emphasizing the high spatial frequencies of the stimulus (Henning and Wörgötter, 2007). Importantly, during the course of fixational switches, the change between microscopic tremor and macroscopic eye movements enables a time-varying multiplexing of visual information at different spatial scales (Rucci, 2008). Accordingly, for oscillatory stimulus-locked activity substantially lower than the gamma range, as observed in our study, the system appears flexible as to which channels carry either global or local feature information (Jancke, 2000).

#### Divergent readout of available information in primary visual cortex

In our study we consider the gratings' retinotopic motion as the source of local signals and the gratings' orientation as the prominent global stimulus feature. Such multiple signals may enable the network to differently affect downstream areas: The fast cortical retinotopic propagation might dominate readout in motion sensitive areas that analyze motion speed and solve the 'aperture problem' by integrating motion direction across larger receptive field sizes (Glaser and Barch, 1999; Movshon et al., 1985; Rust et al., 2006; Wallach, 1935; Zhang and Britten, 2006). In parallel, the presence of a steady orientation map signals slowly changing stimulus features (Wiskott and Sejnowski, 2002; Wyss et al., 2006) to enable invariant representation at higher visual processing stages engaged in form representation (Karklin and Lewicki, 2009). Finally, such complex spatio-temporal activity dynamics could play an important role in cortical memory consolidation particularly, when dealing with high-dimensional natural input (Yao et al., 2007).

Supplementary materials related to this article can be found online at doi:10.1016/j.neuroimage.2011.01.004.

#### Acknowledgments

We thank Ulf T. Eysel, Hubert R. Dinse, Benedict Ng, and John Lipinski for helpful comments on the manuscript. We thank Winfried Junke, Stefan Dobers and the mechanical shop of the Ruhr-University Bochum for excellent technical support. The work was financially supported by the BMBF (D.J.) and SFB Neurovision 509 (Hoffmann K.-P. and Distler C.).

#### References

- Abeles, M., 1991. Corticonics. Cambridge Univ. Press, Cambridge. 482
- Ahissar, E., Arieli, A., 2001. Figuring space by time. Neuron 32, 185–201. 483
- Ahmed, B., Hanazawa, A., Undeman, C., Eriksson, D., Valentiniene, S., Roland, P.E., 2008. Cortical dynamics subserving visual apparent motion. Cereb. Cortex 18, 2796–2810. 484
- Aubry, N., Guyonnet, R., Lima, R., 1991. Spatiotemporal analysis of complex signals: theory and applications. J. Stat. Phys. 64, 683–739. 485
- Abeles, M., Goldstein, M.H., 1977. Multispike train analysis. Proc. IEEE 65, 762–773. 486
- Basole, A., White, L.E., Fitzpatrick, D., 2003. Mapping multiple features in the population response of visual cortex. Nature 423, 986–990. 487
- Benucci, A., Frazor, R.A., Carandini, M., 2007. Standing waves and traveling waves distinguish two circuits in visual cortex. Neuron 55, 103–117. 488
- Blasdel, G.G., Salama, G., 1986. Voltage-sensitive dyes reveals a modular organization in the monkey striate cortex. Nature 321, 579–585. 489
- Bonhoeffer, T., Grünvald, A., 1991. Iso-orientation domains in cat visual cortex are arranged in pinwheel-like patterns. Nature 353, 429–431. 490
- Bosking, W.H., Zhang, Y., Schofield, B., Fitzpatrick, D., 1997. Orientation selectivity and arrangement of horizontal connections in tree shrew striate cortex. J. Neurosci. 17, 2112–2127. 491
- Bosking, W.H., Crowley, J.C., Fitzpatrick, D., 2002. Spatial coding of position and orientation in primary visual cortex. Nat. Neurosci. 5, 874–882. 492
- Buzas, P., Volgushev, M., Eysel, U.T., Kisvarday, Z.F., 2003. Independence of visuotopic representation and orientation map in the visual cortex of the cat. Eur. J. Neurosci. 18, 957–968. 493
- Das, A., Gilbert, C.D., 1997. Distortions of visuotopic map match orientation singularities in primary visual cortex. Nature 387, 594–598. 494
- Engel, S.A., Rumelhart, D.E., Wandell, B.A., Lee, A.T., Glover, G.H., Chichilnisky, E.J., Shadlen, M.N., 1994. fMRI of human visual cortex. Nature 369, 525. 495

- Engel, S.A., Glover, G.H., Wandell, B.A., 1997. Retinotopic organization in human visual cortex and the spatial precision of functional MRI. *Cereb. Cortex* 7, 181–192.
- Glaser, E.M., Ruchkin, D.S., 1976. Evoked potentials: principal components and varimax analysis. In: Glaser, E.M., Ruchkin, D.S. (Eds.), *Principles of Neurobiological Signal Analysis*. Academic, New York, pp. 233–290.
- Glaser, D.A., Barch, D., 1999. Motion detection and characterization by an excitable membrane: the “bow wave” model. *Neurocomputing* 26–27, 137–146.
- Grinvald, A., Frostig, R.D., Lieke, E.E., Hildesheim, R., 1988. Optical imaging of neuronal activity. *Physiol. Rev.* 68, 1285–1366.
- Grinvald, A., Lieke, E.E., Frostig, R.D., Hildesheim, R., 1994. Cortical point-spread function and long-range lateral interactions revealed by real-time optical imaging of macaque monkey primary visual cortex. *J. Neurosci.* 14, 2545–2568.
- Grinvald, A., Hildesheim, R., 2004. VSDI: a new era in functional imaging of cortical dynamics. *Nat. Rev. Neurosci.* 5, 874–885.
- Gray, C.M., König, P., Engel, A.K., Singer, W., 1989. Oscillatory responses in cat visual cortex exhibit inter-columnar synchronization which reflects global stimulus properties. *Nature* 338, 334–337.
- Henning, M.H., Wörgötter, F., 2007. Effects of fixational eye movements on retinal ganglion cell responses: a modelling study. *Front. Comput. Neurosci.* 1, 2.
- Hubel, D.H., Wiesel, T.N., 1959. Receptive fields of single neurons in the cat's striate cortex. *J. Physiol.* 148, 574–591.
- Hubel, D.H., Wiesel, T.N., 1974. Sequence regularity and geometry of orientation columns in the monkey striate cortex. *J. Comp. Neurol.* 158, 267–293.
- Hübener, M., Shoham, D., Grinvald, A., Bonhoeffer, T., 1997. Spatial relationships among three columnar systems in cat area 17. *J. Neurosci.* 17, 9270–9284.
- Issa, N.P., Rosenberg, A., Husson, T.R., 2008. Models and measurements of functional maps in V1. *J. Neurophys.* 99, 2745–2754.
- Jancke, D., 2000. Orientation formed by a spot's trajectory: a two-dimensional population approach in primary visual cortex. *J. Neurosci.* 20, RC86.
- Jancke, D., Chavane, F., Naaman, S., Grinvald, A., 2004. Imaging cortical correlates of illusion in early visual cortex. *Nature* 428, 423–426.
- Jin, J.Z., Weng, C., Yeh, C.I., Gordon, J.A., Ruthazer, E.S., Stryker, M.P., Swadlow, H.A., Alonso, J.M., 2008. On and off domains of geniculate afferents in cat primary visual cortex. *Nat. Neurosci.* 11, 88–94.
- Jung, T.P., Makeig, S., Westerfield, M., Townsend, J., Courchesne, E., Sejnowski, T.J., 2000. Removal of eye activity artifacts from visual event-related potentials in normal and clinical subjects. *Clin. Neurophysiol.* 111, 1745–1758.
- Karklin, Y., Lewicki, M.S., 2009. Emergence of complex cell properties by learning to generalize in natural scenes. *Nature* 457, 83–86.
- Kaysner, C., Montemurro, M.A., Logothetis, N.K., Panzeri, S., 2009. Spike-phase coding boosts and stabilizes information carried by spatial and temporal spike patterns. *Neuron* 61, 597–608.
- Koepsell, K., Wang, X., Vaingankar, V., Wie, Y., Wang, Q., Rathbun, D.L., Usrey, W.M., Hirsch, J.A., Sommer, F.T., 2009. Retinal oscillations carry visual information to cortex. *Front. Syst. Neurosci.* 3, 4.
- Koepsell, K., Wang, X., Hirsch, J.A., Sommer, F.T., 2010. Exploring the function of neural oscillations in early sensory systems. *Front. Neurosci.* 4, 53–61.
- Lee, S.H., Blake, R., Heeger, D.J., 2005. Traveling waves of activity in primary visual cortex during binocular rivalry. *Nat. Neurosci.* 8, 22–23.
- Maffei, L., Fiorentini, A., 1973. The visual cortex as a spatial frequency analyser. *Vis. Res.* 13, 1255–1267.
- Mante, V., Carandini, M., 2003. Visual cortex: seeing motion. *Curr. Biol.* 13, R906–R908.
- Movshon, J.A., Thompson, I.D., Tolhurst, D.J., 1978a. Receptive field organization of complex cells in the cat's striate cortex. *J. Physiol.* 283, 79–99.
- Movshon, J.A., Thompson, I.D., Tolhurst, D.J., 1978b. Spatial and temporal contrast sensitivity of neurones in areas 17 and 18 of the cat's visual cortex. *J. Physiol.* 283, 101–120.
- Movshon, J.A., Adelson, E.H., Gizzi, M.S., Newsome, W.T., 1985. The analysis of moving visual patterns. In: Chagas, C., Gattass, R., Gross, C. (Eds.), *Pattern Recognition Mechanisms*. Pontificia Academia Scientiarum, Vatican City, pp. 117–151.
- Petersen, C.C., Grinvald, A., Sakmann, B., 2003. Spatiotemporal dynamics of sensory responses in layer 2/3 of rat barrel cortex measured in vivo by voltage-sensitive dye imaging combined with whole-cell voltage recordings and neuron reconstructions. *J. Neurosci.* 23, 1298–1309.
- Pollen, D.A., Andrews, B.W., Feldon, S.E., 1978. Spatial frequency selectivity of periodic complex cells in the visual cortex of the cat. *Vis. Res.* 18, 665–682.
- Prechtl, J.C., Cohen, L.B., Pesaran, B., Mitra, P.P., Kleinfeld, D., 1997. Visual stimuli induce waves of electrical activity in turtle cortex. *Proc. Natl Acad. Sci. USA* 94, 7621–7626.
- Reynaud, A., Takerkart, S., Masson, G.S., Chavane, F., 2011. Linear model decomposition for voltage-sensitive dye imaging signals: application in awake behaving monkey. *Neuroimage* 54, 1196–1210.
- Richmond, B., Optican, L., Spitzer, H., 1990. Temporal encoding of two-dimensional patterns by single units in primate primary visual cortex. I. Stimulus-response relations. *J. Neurophysiol.* 64, 351–369.
- Roelfsema, P.R., Lamme, V.A., Spekreijse, H., 2004. Synchrony and covariation of firing rates in the primary visual cortex during contour grouping. *Nat. Neurosci.* 7, 982–991.
- Ross, W.N., Salzberg, B.M., Cohen, L.B., Grinvald, A., Davila, H.V., Waggoner, A.S., Wang, C.H., 1977. Changes in absorption, fluorescence, dichroism, and birefringence in stained giant axons: optical measurement of membrane potential. *J. Membr. Biol.* 33, 141–183.
- Rucci, M., 2008. Fixational eye movements, natural image statistics, and fine spatial vision. *Network* 19, 253–285.
- Rust, N.C., Mante, V., Simoncelli, E.P., Movshon, J.A., 2006. How MT cells analyze the motion of visual patterns. *Nat. Neurosci.* 9, 1421–1431.
- Senseman, D.M., Robbins, K.A., 1999. Modal behavior of cortical neural networks during visual processing. *J. Neurosci.* 19 (RC3), 1–7.
- Sharon, D., Grinvald, A., 2002. Dynamics and constancy in cortical spatiotemporal patterns of orientation processing. *Science* 295, 512–515.
- Sharon, D., Jancke, D., Chavane, F., Na'aman, S., Grinvald, A., 2007. Cortical response field dynamics in cat visual cortex. *Cereb. Cortex* 17, 2866–2877.
- Shoham, D., Hübener, M., Schulze, S., Grinvald, A., Bonhoeffer, T., 1997. Spatio-temporal frequency domains and their relation to cytochrome oxidase staining in cat visual cortex. *Nature* 385, 529–533.
- Sirovich, L., 1987. Turbulence and the dynamics of coherent structures, Part I. Coherent structures, Part II. Symmetries and transformations, Part III. Dynamics and scaling. *Q. Appl. Math.* 45, 561–590.
- Sirovich, L., Everson, R., Kaplan, E., Knight, B.W., O'Brien, E., Orbach, D., 1996. Modeling the functional organization of the visual cortex. *Phys. D* 96, 355–366.
- Sornborger, A., Sailstad, C., Kaplan, E., Sirovich, L., 2003. Spatiotemporal analysis of optical imaging data. *Neuroimage* 18, 610–621.
- Strang, G., 2007. *Computational Science and Engineering*. Wellesley-Cambridge Press.
- Tusa, R.J., Palmer, L.A., Rosenquist, A.C., 1978. The retinotopic organization of area 17 (striate cortex) in the cat. *J. Comp. Neurol.* 177, 213–236.
- Wallach, H., 1935. Über visuell wahrgenommene Bewegungsrichtung. *Psychol. Forsch.* 20, 25–380.
- Wiskott, L., Sejnowski, T., 2002. Slow feature analysis: unsupervised learning of invariances. *Neural Comp.* 14, 715–770.
- Wyss, R., König, P., Verschure, P.F., 2006. A model of the ventral visual system based on temporal stability and local memory. *PLoS Biol.* 4, e120.
- Xu, X., Collins, C.E., Khaytin, L., Kaas, J.H., Casagrande, V.A., 2006. Unequal representation of cardinal vs. oblique orientations in the middle temporal visual area. *Proc. Natl Acad. Sci. USA* 103, 17490–17495.
- Yacoub, E., Harel, N., Ugurbil, K., 2008. High-field fMRI unveils orientation columns in humans. *Proc. Natl Acad. Sci. USA* 105, 10607–10612.
- Yao, H., Shi, L., Han, F., Gao, H., Dan, Y., 2007. Rapid learning in cortical coding of visual scenes. *Neuron* 10, 772–778.
- Yeh, C.-I., Xing, D., Shapley, R.M., 2009. “Black” responses dominate Macaque primary visual cortex V1. *J. Neurosci.* 29, 11753–11760.
- Yu, H., Farley, B.J., Jin, D.Z., Sur, M., 2005. The coordinated mapping of visual space and response features in visual cortex. *Neuron* 47, 267–280.
- Zhang, T., Britten, K.H., 2006. The virtue of simplicity. *Nat. Neurosci.* 9, 1356–1357.